NIH Public Access

Author Manuscript

Sens Actuators A Phys. Author manuscript; available in PMC 2011 July 1.

Published in final edited form as:
Sens Actuators A Phys. 2010 July 1; 162(1): 130–136. doi:10.1016/j.sna.2010.06.011.

A Wafer-Scale Etching Technique for High Aspect Ratio Implantable MEMS Structures

R Bhandari*, **S Negi**, **L. Rieth**, and **F Solzbacher**
Dept of Electrical and Computer Engineering, University of Utah 50 South Central Campus Drive, Salt Lake City, UT 84112, USA

Abstract

Microsystem technology is well suited to batch fabricate microelectrode arrays, such as the Utah electrode array (UEA), intended for recording and stimulating neural tissue. Fabrication of the UEA is primarily based on the use of dicing and wet etching to achieve high aspect ratio (15:1) penetrating electrodes. An important step in the array fabrication is the etching of electrodes to produce needle-shape electrodes with sharp tips. Traditional etching processes are performed on a single array, and the etching conditions are not optimized. As a result, the process leads to variable geometries of electrodes within an array. Furthermore, the process is not only time consuming but also labor-intensive. This report presents a wafer-scale etching method for the UEA. The method offers several advantages, such as substantial reduction in the processing time, higher throughput and lower cost. More importantly, the method increases the geometrical uniformity from electrode to electrode within an array (1.5 ± 0.5 % non-uniformity), and from array to array within a wafer (2 ± 0.3 % non-uniformity). Also, the etching rate of silicon columns, produced by dicing, are studied as a function of temperature, etching time and stirring rate in a nitric acid rich HF-HNO_3 solution. These parameters were found to be related to the etching rates over the ranges studied and more-importantly affect the uniformity of the etched silicon columns. An optimum etching condition was established to achieve uniform shape electrode arrays on wafer-scale.

Keywords

Utah electrode array (UEA); neural interface; HF-HNO_3 wet etching; high aspect ratio; microelectrodes

1. Introduction

A major design parameter for neural interfaces is the electrode geometry [1-7]. The geometrical characteristics of individual electrodes influence many of the electrical properties (impedance, capacitance, etc.) [6]. Thus uniformity of electrode geometry over each array is important. Furthermore, the penetrating electrodes in an implanted array must compromise as little cortical volume as possible (ideally zero). Thus each electrode must be made as slender as possible, and should have sharp tips (< 1 μm diameter) and be sufficiently long to be able to reach neurons, yet retain sufficient strength to withstand the

© 2010 Elsevier B.V. All rights reserved.

*Corresponding author: Rajmohan Bhandari, r.bhandari@utah.edu.

Publisher's Disclaimer: This is a PDF file of an unedited manuscript that has been accepted for publication. As a service to our customers we are providing this early version of the manuscript. The manuscript will undergo copyediting, typesetting, and review of the resulting proof before it is published in its final citable form. Please note that during the production process errors may be discovered which could affect the content, and all legal disclaimers that apply to the journal pertain.

NIH-PA Author Manuscript NIH-PA Author Manuscript NIH-PA Author Manuscript

NIH-PA Author Manuscript

NIH-PA Author Manuscript

NIH-PA Author Manuscript

implantation procedure. Also, the electrode should have a cylindrical geometry (or slightly conical) so that they induce minimum tissue inflammation [8-9]. It is desirable to minimize the engineering tolerances (variation in electrode geometry from array to array) so that one can reliably interpret the observed variations in physiological results.

The UEA consists of 100 microelectrodes, which are 1.5 mm in length, supported by a 0.5 mm back plane. Fig. 1 shows a cartoon image of the UEA. The electrodes of the UEA are electrically isolated from each other by a moat of glass that surrounds the base of each electrode [6-7]. The UEA comes in various configurations such as the slant [10] and the convoluted electrode arrays [11]. An important and early step in the array fabrication is the etching of electrodes to produce needle-shape electrodes with sharp tips. Etching of the UEA has two-steps consisting of (1) *dynamic* and (2) *static* etching [6]. Square columns are fabricated by dicing and are subsequently transformed into rounded and pointed electrodes through a wet etching process (mixture of HF (49%)-HNO_3 (69%) in a ratio of 1:19 by volume) that rounds the column corners and sharpens the tip. Traditional etching processes are performed on a single array, and the etching conditions are not optimized resulting in variable geometries of electrodes within an array. Furthermore, the process is not only time consuming but also labor-intensive. In order to achieve geometrical uniformity in electrodes, a wafer-scale etching method was developed and optimum etching conditions were investigated in this paper.

The wet etching of silicon with HF-HNO_3 mixtures is widely used in the semiconductor industry and in the production of solar cells [12-17]. This etch process is employed for the removal of work damage or roughness (e.g., caused by sawing of wafers), for the planar removal of silicon, or for texturing of the surface [13]. A detailed study of the etching mechanism was done by Robbins and Schwartz for planar silicon surfaces [12-15]. In the literature, the etching of silicon in HF-HNO_3 mixtures is described as two-step chemical process that includes (1) oxidation of Si to SiO_2 by nitric acid (Eq. 1) and (2) etching of SiO_2 by HF (Eq. 2). The overall reaction is given in Eq. 3.

$$3Si+4HNO_3 \rightarrow 3SiO_2+4NO\uparrow+2H_2O \quad (1)$$

$$SiO_2+6HF \rightarrow H_2SiF_6+2H_2O \quad (2)$$

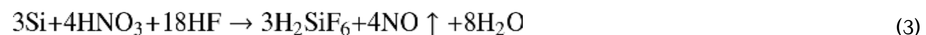

$$3Si+4HNO_3+18HF \rightarrow 3H_2SiF_6+4NO\uparrow+8H_2O \quad (3)$$

The crucial step in this reaction is the oxidation of silicon by nitric acid. For isotropic etching involving HF-HNO_3, water or acetic acid (etchant popularly known as HNA) are used as diluents to modify the rate of reaction, finish of the etched surface, or to cause preferential etching of certain crystallographic planes [12-15]. The topography of the etched silicon surface depends on the composition of the etch solution. In the literature, iso-etch curves for various weight percentages of the constituents for an HF-HNO_3 system have been reported [15]. The ratio between HF, HNO_3 and diluents determines if the etching is diffusion limited or reaction limited. Furthermore, the etch rate is higher in convex corners resulting in the development of rounded corners and edges [15]. If diluent is added, the reaction becomes reaction rate-limited, leading to decrease in etch rate and sharp peaked corners and edges [15]. To make smooth and rounded electrodes it is important to have dissolution step (Eq. 2) as diffusion limited [12-15]. Thus this study was limited to nitric acid rich HF (49%)-HNO_3 (69%) system in a ratio of 1:19 by volume.

NIH-PA Author Manuscript NIH-PA Author Manuscript NIH-PA Author Manuscript

2. Method

2.1. Dicing

A 2 mm thick, 75 mm diameter *p*-type, c-Si (100) wafer with a resistivity of 0.01-0.05 Ω-cm were used as substrates. A Disco dicing saw, DAD 640, is used to cut two orthogonal sets of deep kerfs into the silicon wafer. Vertical columns were formed in each array by making 13 cuts of 1.5 mm depth with an index of 0.4 mm. The wafer was then rotated by 90° and an additional 13 cuts were made with the same parameters. The thirteen cuts yielded 10 rows of electrodes plus one extra row of electrodes on all four sides of the array. The saw leaves a 0.5 mm thick substrate at the base of the cuts. Depending on the size of the wafer large number of arrays can be accommodated. The average column width after dicing was 240 ± 15 μm. Apart from the extra row of electrodes, the *fins* and the *corner posts* were fabricated, as shown in Fig. 2. The extra row of electrodes, *fins* and the *corner posts* were designed to enhance uniformity in electrode geometry across the array during wet etching. There were 49 arrays in a wafer.

2.2. Wafer-scale etching

The wafer-scale etching concept is similar to traditional UEA etching and has two-steps consisting of (1) *dynamic* and (2) *static* etching [6]. Fig. 3 (A-D) illustrates the etching principle. A 100 mm diameter Teflon wafer holder was developed for wafer-scale wet etching of the 75 mm diameter diced wafers containing 49 arrays. The wafer holder comprised of two components: a top plate and a base plate. The base plate has a 75 mm diameter recess and contains an O-ring. The wafer snugly sits on this recess and the O-ring protects the backside of the wafer from the wet etchant. Fig. 4 presents a photograph of the wafer holder. The top plate consists of a hollow Teflon retaining ring that was made to hold the wafer in place. The top plate is attached to the base plate with the help of six Teflon screws. The wafer holder has a threaded hole to allow the holder to be fixed into the etching apparatus.

In the *dynamic* etching, the wafer is mounted in the Teflon wafer holder, and is immersed with columns facing down, into 1500 ml of acid mixture of HF (49%)-HNO_3 (69%) in a ratio of 1:19. Fig. 5 (a) presents a photograph of the *dynamic* wafer scale etching setup. The wafer holder is rotated clockwise (22 rpm) while the magnetic stirrer, rotating counter-clockwise, stirs the acid aggressively. The unique combination of wafer and stir-bar rotation causes an aggressive and continuous flow of the etchant into the high aspect ratio columns, thereby leading in uniform etching across the side-walls of the square columns. The important dynamic etching parameters are separation between the magnetic stir-bar and wafer (fixed to 2 inches in this study), agitation or rotation rate of the etching solution, temperature of the etching solution (because of exothermic reaction of HF and HNO_3 with silicon) and the etching time. Thus the etch rate of silicon columns, produced by dicing, was studied as a function of temperature, etching time and stirring rate and described in detail in following section. During the *static* etching process the holder is placed in 750ml of acid mixture with the columns facing upwards, and neither the acid is stirred nor is the wafer rotated. Fig. 5(b) presents a photograph of *static* wafer-scale etching setup. A custom designed Teflon jig was built to continuously vent the gas evolved during *static* etching. The hollow jig has through holes on one side and is connected to a compressed air cylinder through plastic tubing. The *static* etch preferentially etches and sharpens the tops of the columns, until the final column shape has a sharp tip. The etch rate is greater at the tops of the columns because the activity of the etching solution at the base of microneedle is reduced, and little fluid motion is present to replenish it.

NIH-PA Author Manuscript
NIH-PA Author Manuscript
NIH-PA Author Manuscript

2.1. Agitation

An experiment was carried out to examine the affect of agitation on the etch rate and uniformity of electrode during *dynamic* etching. A 2.5 inch stir-bar was used and the rotation rate was varied from 100 to 700 rpm. Wafers were diced by the described method. Etching was carried out each time for 4 min. To characterize the etch rate (μm/min) and non-uniformity (%), the dimensions (length and width) at the top of the columns in each array were measured in optical microscope using *QCapture* software. Fifteen arrays were measured in each wafer. The percentage variation or non-uniformity in electrode tip measurement was calculated as standard deviation multiplied by 100 and divided by the mean.

2.2. Temperature

The affect of temperature on the etch rate and non-uniformity was investigated by performing a experiment where the rotation speed of the stir-bar was fixed to 500 rpm. Test wafers were diced by the method described above. 1500 ml of etching solution was taken each time and the temperature was varied from 20-60 C .The wafers were etched for 4 min each time. After etching, the tops of several columns were measured in an optical microscope using *QCapture* software, and the non-uniformity in the electrode width was calculated.

2.3. Etching time

To study the affect of time on the etch rate and uniformity a experiment was carried out where the rpm of the stir-bar was fixed to 500 rpm. Test wafers were diced by the method described above; 1500 ml of etching solution was taken each time and the etching was carried out for 12 min. The temperature of the etching solution was monitored every 2 min.

3. Results

3.1 Agitation

Agitation helps in maintaining the concentration of the reactants and the product uniform throughout the solution thereby bringing more reactants to the silicon surface and removing products including nitrous oxide bubbles from the surface. Stirring the acid solution creates an aggressive and continuous flow of the etchant into the dicing kerfs, to generate isotropically etched square columns with rounded corners. Nitrous oxide bubbles trapped between the rectangular silicon columns would prevent etching at those locations and cause non-uniform etching in the side-walls of silicon columns. Fig. 6 presents a plot of the relationship obtained empirically between etch rate and non-uniformity in electrode geometry versus agitation (rpm) of the etching solution. Initially (from 100-500 rpm), the etch rate increases linearly with increasing spin-bar speed and then saturates with rpm, while the non-uniformity in electrode geometry decreases initially and then becomes constant with increasing rpm. At 500 rpm the nonuniformity was found to be minimum (<1 %) and therefore was used as a standard for dynamic etching.

Since the etching is performed in low HF and high HNO_3 system (1:19 by volume), the surface of the silicon column will be covered with an oxide layer, due to the abundance of oxidizing agent. Under this condition the rate of silicon removal will be diffusion-limited i.e. the arrival of HF at the SiO_2 surface [12-15]. HF will be consumed immediately at the surface leading to zero concentration at the surface of the silicon column. Thus a concentration gradient of HF will develop between the silicon columns and bulk the etchant as highlighted in Fig. 7. The HF concentration at the silicon interface will be directly related to the thickness of the diffusion layer (δ). The thickness of diffusion layers is known to be

NIH-PA Author Manuscript

NIH-PA Author Manuscript

NIH-PA Author Manuscript

related inversely to the velocity of the reacting species at the interface with respect to the bulk of the solution [15].

As the stir-bar rotation rate (rpm) increases, the mobility of reactants/products increases, increasing the diffusivity of the etchants, as a result the etch rate increases. Since the HF-HNO_3 reaction is known to be exothermic [12], an increase in etch rate would cause increase in heat of reaction leading to increase temperature of etchant. An increase in temperature of the solution, in-turn increases the diffusion coefficient of the etchant, causing an increase in the etch rate which will increase the etchant temperature, resulting in a positive feedback. The non-uniformity decreases with increasing rotation rate and then becomes constant because the temperature becomes a dominant factor and starts influencing the etch rate. After some time the etch rate saturates because the temperature of the etching bath achieves thermal equilibrium with the environment.

3.2. Temperature

The heat of reaction sets up thermal gradient in the vicinity of the specimen and therefore causes the diffusion coefficient to become a function of the distance from the reacting surface. There is a thermal gradient, because of the flow of heat of reaction away from the surface. The temperature profile is proportional to the amount of heat generated which in-turn is controlled by reaction rate. The thermal gradient causes a distortion in the concentration profile making it steeper, as shown in Fig. 7, and thus enhanced reaction rates. Fig. 8 presents a plot of etch rate and non-uniformity (%) in tip geometry as a function of reciprocal of the etchant temperature. As depicted in the graph, as the temperature of the etchant increases, the etch rate increases exponentially and the non-uniformity is more pronounced.

3.3. Etching time

Diffusion-controlled etch processes lead to development of rounded corners and edges, since the availability of reagent is greater at the corners and edges of the specimen than at the center (oxidation step ceases to be rate determining) [14]. Fig. 9 shows the plot between temperature of the etchant and etching time. As etching time increases temperature of etchant monotonically increases and approaches a saturation value. As the etching progresses, the rectangular columns first isotropically etch, decreasing the column dimensions and generating rounded corners, and then transform into sharp pointed electrodes. Fig. 10 illustrates the etching progression. The electrodes are desired to be slender in shape, ideally longer *dynamic* etching time is preferred however, as mentioned previously, as the etching time increases the effect of temperature becomes dominant, resulting in highly non-uniform electrodes. Therefore, the *dynamic* etching time was limited to 4 min and used as a standard.

4. Discussion

Although electrode materials (for example platinum, iridium oxide, conducting polymers etc.) coated on the tips of the electrode affects the electrical properties such as impedance [18-20], the uniformity in electrical properties is directly influenced by the geometry of the electrodes. Accordingly, the wafer-scale etching technique developed in this work is designed to achieve geometrical uniformity. The optimized etching parameters are listed in Table 1. In order to evaluate the repeatability of the etching process five wafers were etched using the optimized etching conditions highlighted in Table 1. Since the temperature of the etching solution plays an important role in the uniformity of electrode geometry (discussed in section 3.2), for the *static etching*, the 750 ml of acid solution used was divided into two equal halves. The wafer were first etched for 4 min using half of the prepared solution, then

NIH-PA Author Manuscript

again etched for 4 min using the second half of the solution. After static etchings, the five wafers were cross-sectioned using a dicing saw and electrode lengths were measured across each array (7 arrays/wafer) using an optical comparator (Nikon V12A comparator). Table 2. summarizes the etching results obtained in five wafers. The average tip width measured after *dynamic etching* was 122±7μm. The average nonuniformity in tip width was 2 % ± 0.3 across the five wafers. The percentage of non-uniformity within an array was 1.5% ± 0.5. After *static etching*, the non-uniformity in electrode length was 1.1 % ±0.1, while the average electrode length was 1.3 mm. Fig. 11 shows an approximately scaled drawing of an electrode side view showing the three measurement planes where nonuniformity was made.

Fig. 12 shows SEM image of the electrode array after *static etching*. In order to examine the roughness inherited by the wet etching process on the electrode surface, two planar test wafers (no electrodes) were etched using the optimized etching conditions (Table 1.). The roughness (rms) was measured using Zygo NewView 5032, and was found to be 0.84 μm ± .015.

The wafer-scale etching offers several advantages over the conventional array-scale etching including: batch fabrication, greater degree of uniformity in electrode geometry within an array, and high reproducibility. The non-uniformity percentage after dynamic etching across the wafer by wafer-scale etching technique is six times less than the single-array etching, while the non-uniformity in electrode length , after static etching, is six times less while width is ten times. More importantly the wafer-scale etching fabricates electrode columns with rounded corners, with a smooth and slightly positive tapered tip (column that narrows at the top). The importance of such features has not been quantified but may have significance in pushing the tissue out of the way instead of cutting during insertion [8-9]. Furthermore, the wafer-scale etching not only increases throughput, but also reduces lead time for etching the UEA. It takes 30 min to etch a 75 wafer diameter wafer comprising of 49 arrays, while to etch the same amount of arrays it would take 25 hours. This reduction in lead time would be critical for volume production of the UEA in future.

The wafer-scale etching along with the photoresist masking process (described in detail elsewhere [21]) lead to reduction in non-uniformity in impedance of the electrode arrays by half. A detailed description of comparison of geometrical and electrical characteristics of the electrode arrays developed by the new wafer-scale UEA fabrication method and the conventional array-scale technique is given elsewhere [22]. The arrays are removed from *fins* and *corner post* and singulated into 10 × 10 electrode arrays by using the dicing saw, a detail description of the process is given in elsewhere [22].

NIH-PA Author Manuscript

5. Conclusion

This paper describes a cost effective, mask-less, wafer-scale method for etching high aspect ratio (15:1) implantable MEMS structures. The technique employs nitric acid rich HF-HNO_3 wet etchant (1:19 by volume) to reproducibly achieve uniform shape electrode arrays. The unique combination of etching parameters significantly increases the etching uniformity within an array and across the wafer. The major advantage of this method compared to other techniques employed for etching high aspect ratio implantable devices is the simplicity of the method. The degree of control achieved in the dimensions of the electrode array make them suitable for neuroprosthetic applications.

Biographies

NIH-PA Author Manuscript

Rajmohan Bhandari received his B.S. and M.S. degrees in physics from Garhwal University, Dehradun, India, in 1996 and 1998. In 2000 he received M.Tech degree in

NIH-PA Author Manuscript

NIH-PA Author Manuscript

NIH-PA Author Manuscript

physics from Indian Institute of Technology (IIT), Delhi-India, with majors in MEMS. He worked in a MEMS foundry in Singapore, as a Product Engineer, from 2001-2004. He worked as a Research Assistant in University of Calgary, Canada from 2004-2005. From 2006 to 2009 he was a research assistant in the Integrated Neural Interface Program (INIP) at University of Utah. In 2009 he received PhD in Electrical Engineering from University of Utah. His dissertation was based on wafer-scale fabrication of penetrating neural microelectrode arrays. From 2008-2009 he worked as a Consultant in Blackrock Microsystems, Salt Lake City, USA. Since 2009 (till date) he is Senior R&D MEMS/ Materials Engineer at Blackrock Microsystems. His research interest includes design, fabrication and testing of implantable microdevices, biocompatible materials, and system integration.

Sandeep Negi received his B.S and M.S degrees in physics from Garhwal University, Dehradun, India, in 1996 and 1998, and his MTech degree in physics from Indian Institute of Technology (IIT), Delhi, India, in 2000. From 2001 to 2004, he worked in CMOS and MEMS industry in Singapore as a product engineer. From 2004 through 2005, he worked as a research assistant in University of Calgary, Calgary, Canada. He received his PhD degree in electrical and computer engineering from University of Utah, Salt Lake City, USA in 2009. In his PhD he worked on the materials and novel processes for effective charge injection at the stimulating electrode/tissue interface for the safe and efficacious neuroprostheses. From 2006 to 2009 he was a research assistant in the Integrated Neural Interface Program (INIP) at University of Utah. Since 2009 till date, he is with Blackrock Microsystems, Salt Lake City, USA, working as a senior MEMS/Materials engineer. His research interest includes the design, fabrication and testing of MEMS and BioMEMS devices and deposition and characterization of thin films.

Loren Rieth received his B.S. degree in Materials Science from The Johns-Hopkins University, Baltimore, MD, in 1994. He received his Ph.D. in Materials Science and Engineering from the University of Florida, Gainesville, FL, in 2001. From 2001 to 2003, he was a Postdoctoral Research Associate at the University of Utah, Salt Lake City, UT, and continued on at the University of Utah as a Research Assistant Professor in Materials Science (2003-2005), and Electrical and Computer Engineering (2004-present). His research is focused on deposition and characterization of thin film materials for sensors (chemical, physical, and biological), MEMS, BioMEMS, and energy production.

Florian Solzbacher received his MSc in electrical engineering from the Technical University Berlin in 1997 and his PhD from the Technical University Ilmenau in 2003. He is Director of the Microsystems Laboratory at the University of Utah and a faculty member in the Departments of Electrical and Computer Engineering, Materials Science and Bioengineering. and he is responsible for the Utah branch office of the Fraunhofer IZM, Germany. Dr. Solzbacher is co-founder of First Sensor Technology GmbH, an established supplier to the automotive and process control industry in the USA, Europe and Asia. He is Chairman of the German Association for Sensor Technology AMA. His work focuses on harsh environment microsystems, sensors and materials. He is author of over 60 scientific and engineering publications and book chapters on MEMS devices, technologies and markets for Harsh Environments. Since 2004 he has been Chairman of Sensor + Test, the world's largest international trade fair and ensemble of conferences for sensors, metrology and testing.

6. References

1. Akin T, Najafi K, Smoke RH, Bradley RM. A micromachined silicon sieve electrode for nerve regeneration applications. IEEE Trans.Biomed, Eng 1994;41:305–313. [PubMed: 8063296]

NIH-PA Author Manuscript NIH-PA Author Manuscript NIH-PA Author Manuscript

2. Edel DJ. A peripheral nerve information transducer for amputees: long-term multichannel recording from rabbit peripheral nerves. IEEE Trans.Biomed, Eng 1986;33:203–214. [PubMed: 3007332]

3. BeMent SL, Wise KD, Anderson DJ, Najafi K, Drake KL. Solid-state electrodes for multichannel multiplexed intracortical neuronal recording. IEEE Trans. Biomed, Eng 1986;33:230–241. [PubMed: 3957372]

4. Blum NA, Carkhuff BG, Charles HK Jr. Edwards RL, Meyer RA. Multisite microprobes for neural recording. IEEE Trans. Biomed. Eng 1991;38:68–74. [PubMed: 2026434]

5. Drake KL, Wise KD, Farraye J, Anderson DJ, BeMent SL. Performance of planar multisite microprobes in recording extracellular single – unit intracortical activity. IEEE Trans. Biomed, Engg 1988;35:719–732.

6. Campbell PK, Jones KE, Huber RJ, Horch KW, Normann RA. A silicon based, three dimensional neural interface: manufacturing processes for an intra cortical electrode array. IEEE Trans. Biomed. Eng 1991;38(38):758–768. [PubMed: 1937509]

7. Jones KE, Campbell PK, Normann RA. A glass / silicon composite intra cortical electrode array. Ann Biomed Eng 1992;20:423–437. [PubMed: 1510294]

8. Edell DJ, Toi V, McNeil VM, Clark LD. Factors influencing the biocompatibility of insertable silicon microshafts in cerebral cortex. IEEE Trans.Biomed .Eng 1992;39:635–643. [PubMed: 1601445]

9. Beard RB, Hung BN, Schmukler R. Biocompatibility considerations at stimulating electrode interfaces. Ann. Biomed. Eng 1992;20:395–410. [PubMed: 1443832]

10. Bhandari, R.; Negi, S.; Reith, L.; Solzbacher, F. Wafer-scale Processed, Low Impedance Neural Arrays with Variable Length Microelectrodes. to appear in Proceedings of Transducers '09; Denver, USA. June 21-25, 2009;

11. Bhandari R, Negi S, Rieth L, Normann RA, Solzbacher F. A Novel Method of Fabricating Convoluted Shaped Electrode Arrays for Neural and Retinal Prosthesis. Sensor & Actuators A Phys 2008;145-146(1-2):123–130.

12. Robbins H, Schwartz B. Chemical etching of silicon I. The system HF, HNO_3, and H_2O. J. Electrochem. Soc 1959;106(6):505–508.

13. Robbins H, Schwartz B. Chemical etching of silicon II. The system HF, HNO_3, and $HC_2H_3O_2$. J. Electrochem. Soc 1960;107(2):108–111.

14. Schwartz B, Robbins H. Chemical etching of silicon III. A temperature study in the acid system. J. Electrochem. Soc 1961;108(4):365–372.

15. Schwartz B, Robbins H. Chemical etching of silicon IV. Etching technology. J. Electrochem. Soc 1976;123(12):1903–1909.

16. Klein DL, Stefan DJ. Controlled etching of silicon in HF-HNO_3 system. J. Electrochem. Soc 1962;109:37–42.

17. Steinert M, Acker J, Henbge A. Experimental studies on the mechanism of wet chemical etching of silicon in HF-HNO3 mixtures. J. Electrochem. Soc 2005;152:C843–C850.

18. Negi S, Bhandari R, Rieth L, Solzbacher F. Effect of sputtering pressure on pulsed-DC sputtered iridium oxide films for neuroprosthetic applications. Sensors and Actuators B: Chemical 2009;137(1):370–378.

19. Negi S, Bhandari R, Rieth L, Solzbacher F. In vitro comparison of sputtered iridium oxide and platinum coated neural implantable microelectrode arrays. Biomedical Materials 2010;5(1)

20. Negi S, Bhandari R, Rieth L, Wagenen RV, Solzbacher F. Neural electrode degradation from continuous electrical stimulation: comparison of sputtered and activated iridium oxide. Journal of Neuroscience Methods 2010;186:8–17. [PubMed: 19878693]

21. Bhandari R, Negi S, Rieth L, Normann RA, Solzbacher F. A novel masking technique for high aspect ratio penetrating microelectrode arrays. Journal of Microengineering and Micromechanics 2009;19:035004.

22. Bhandari, R.; Negi, S.; Normann, RA.; Solzbacher, F. Wafer scale fabrication of penetrating neural electrode arrays. Biomedical Microdevices. submitted in

NIH-PA Author Manuscript

NIH-PA Author Manuscript

NIH-PA Author Manuscript

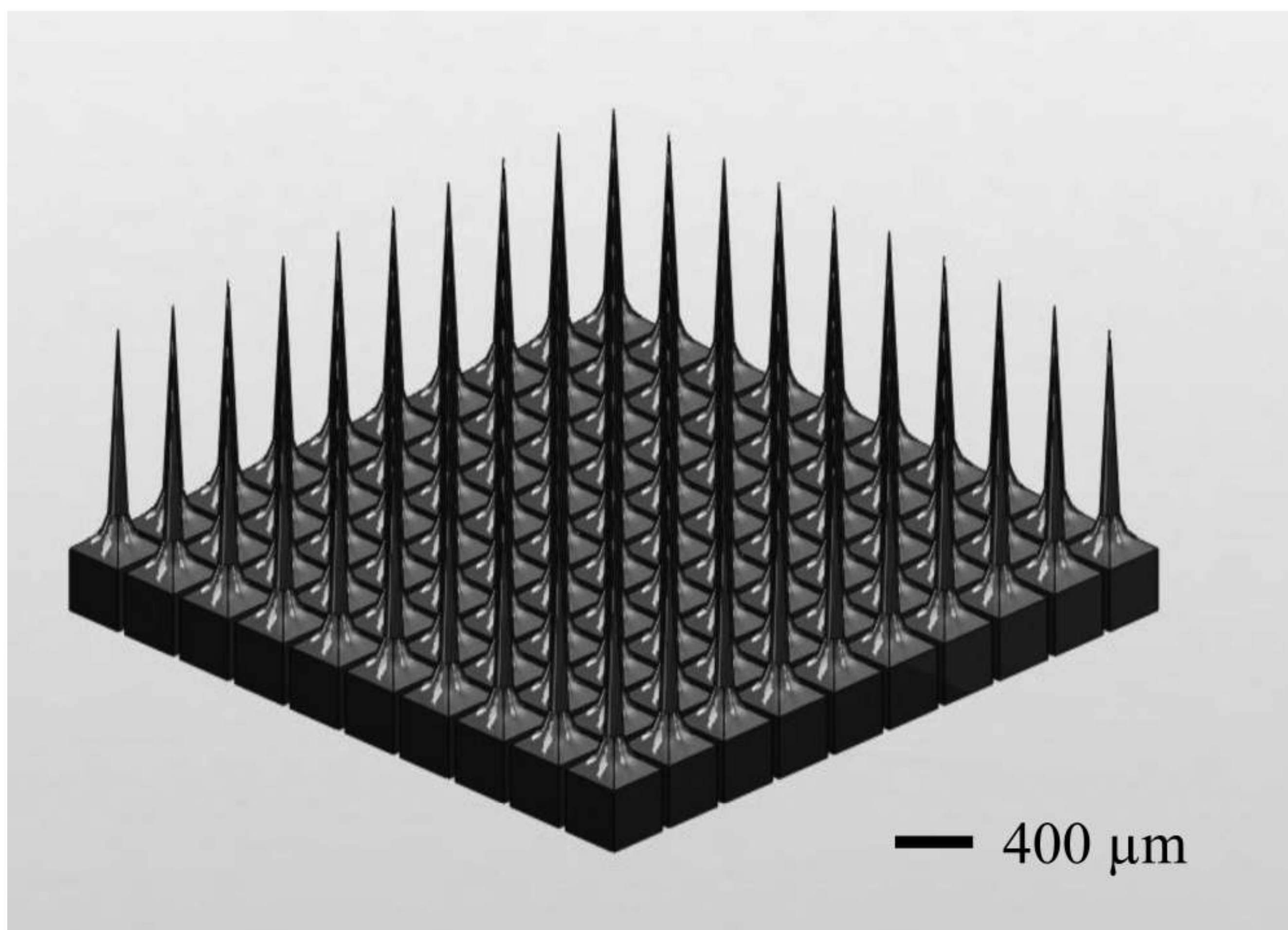

Fig. 1.
Cartoon image of the Utah electrode array.

NIH-PA Author Manuscript
NIH-PA Author Manuscript
NIH-PA Author Manuscript

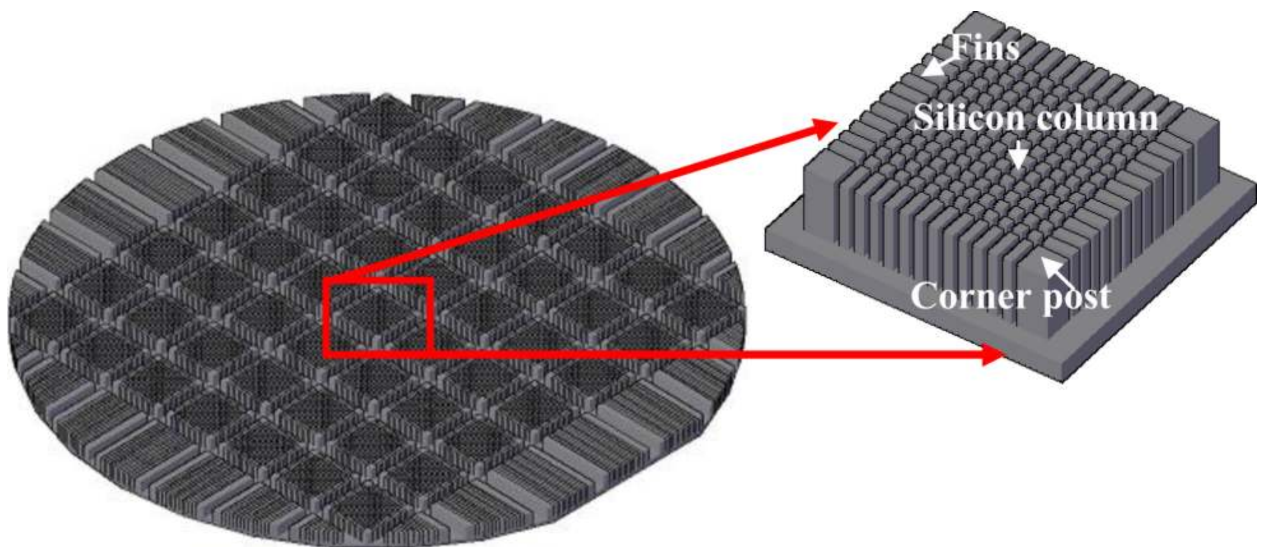

Fig. 2.
Schematic illustration of a wafer containing arrays after using a dicing saw to make 1.5 mm cuts into the silicon wafer. For scale, the length of the columns is 1.5 mm.

NIH-PA Author Manuscript

NIH-PA Author Manuscript

NIH-PA Author Manuscript

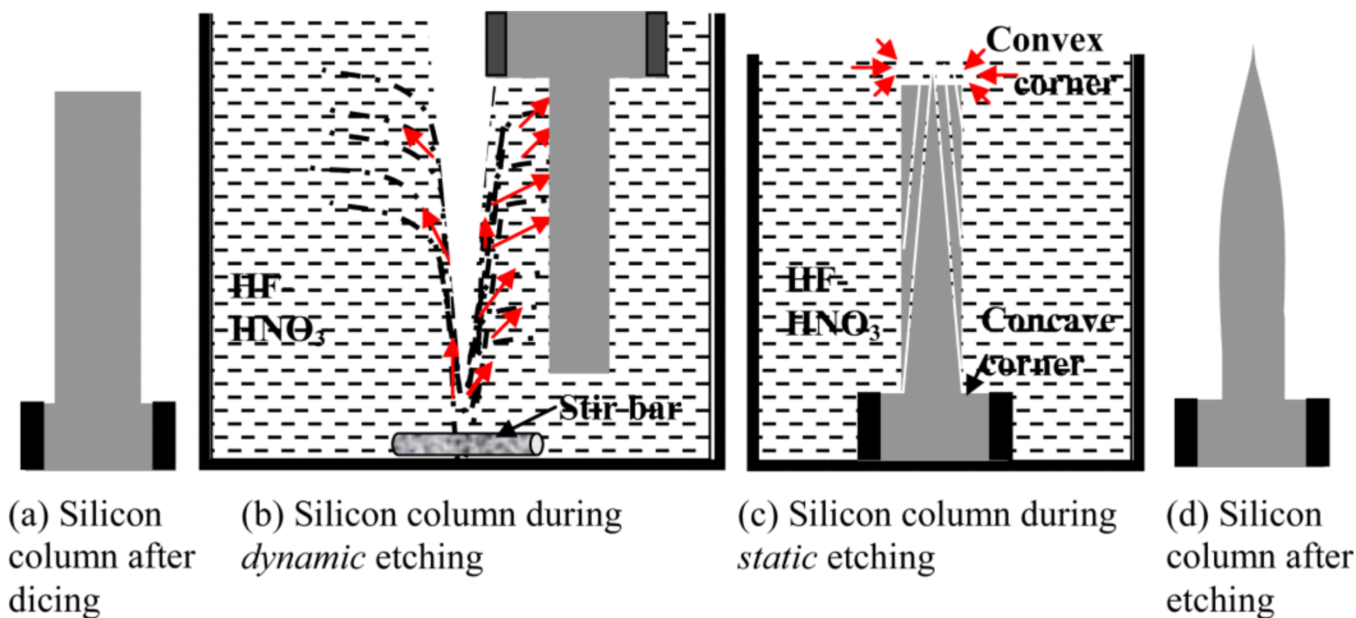

Fig. 3.

Cartoon image of the etching concept. Dicing saw is used to make orthogonal cuts in 2 mm thick silicon wafer to yield 1.5 mm long columns (a). A two step wet etching technique is used, where in the first step (b), called *dynamic* etching, the width of the columns is isotropically thinned, and in the second step (c), called *static* etching, the tips of the electrodes are preferentially sharpened. The arrows indicate pronounced etching.

NIH-PA Author Manuscript
NIH-PA Author Manuscript
NIH-PA Author Manuscript

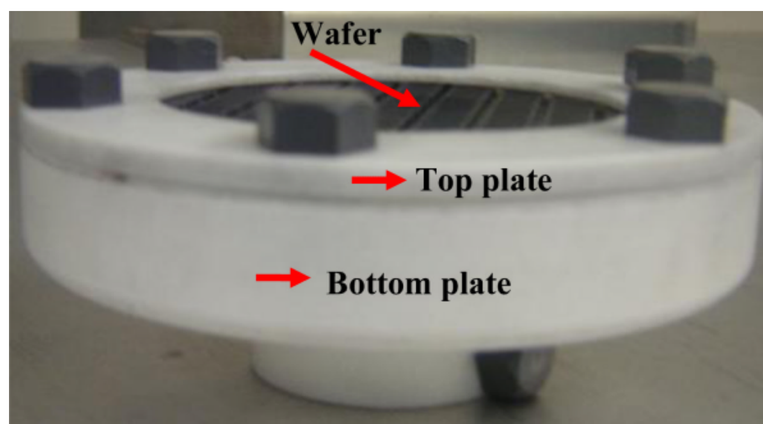

Fig. 4.
Photograph of the custom Teflon wafer holder for wafer- scale etching of electrode arrays.

NIH-PA Author Manuscript
NIH-PA Author Manuscript
NIH-PA Author Manuscript

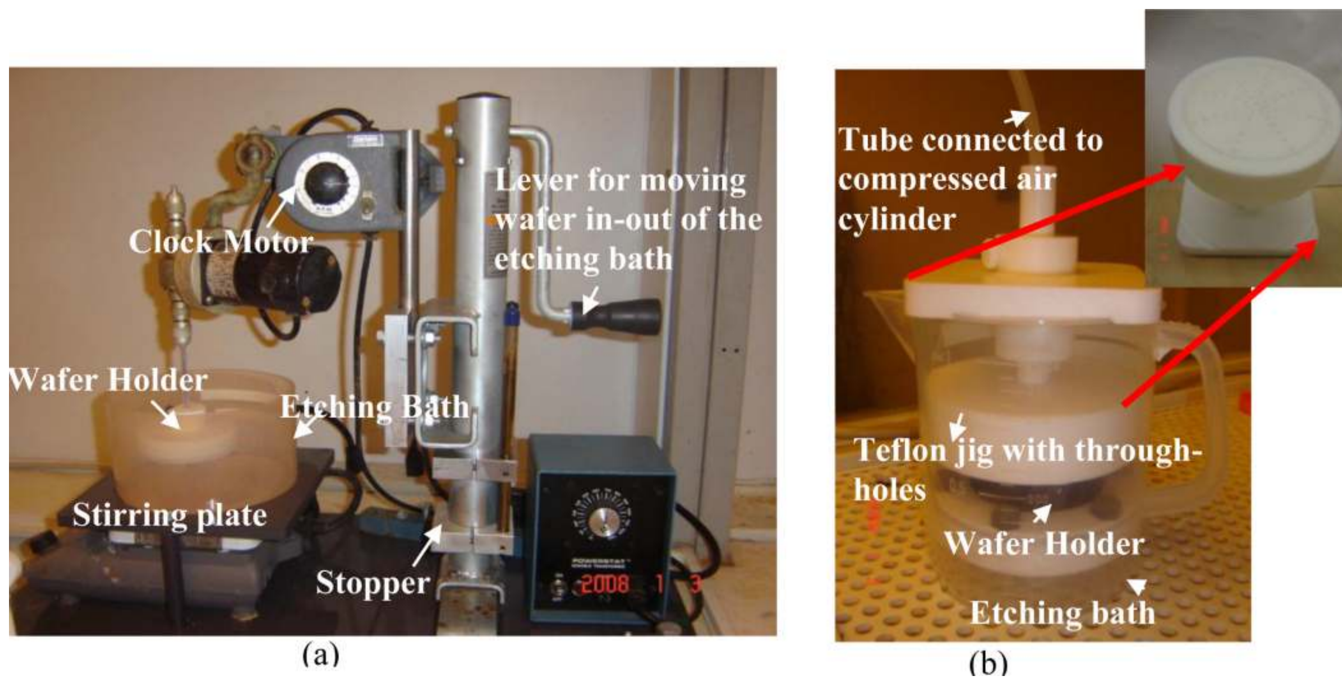

Fig. 5.

Photographs of the wafer scale etching system. (a) Shows *dynamic* etching setup, the width of the columns is isotropically thinned by the aggressive flush of acid. (b) Shows *static* etching setup, the tips of the electrodes are sharpened by the preferential etching.

NIH-PA Author Manuscript

NIH-PA Author Manuscript

NIH-PA Author Manuscript

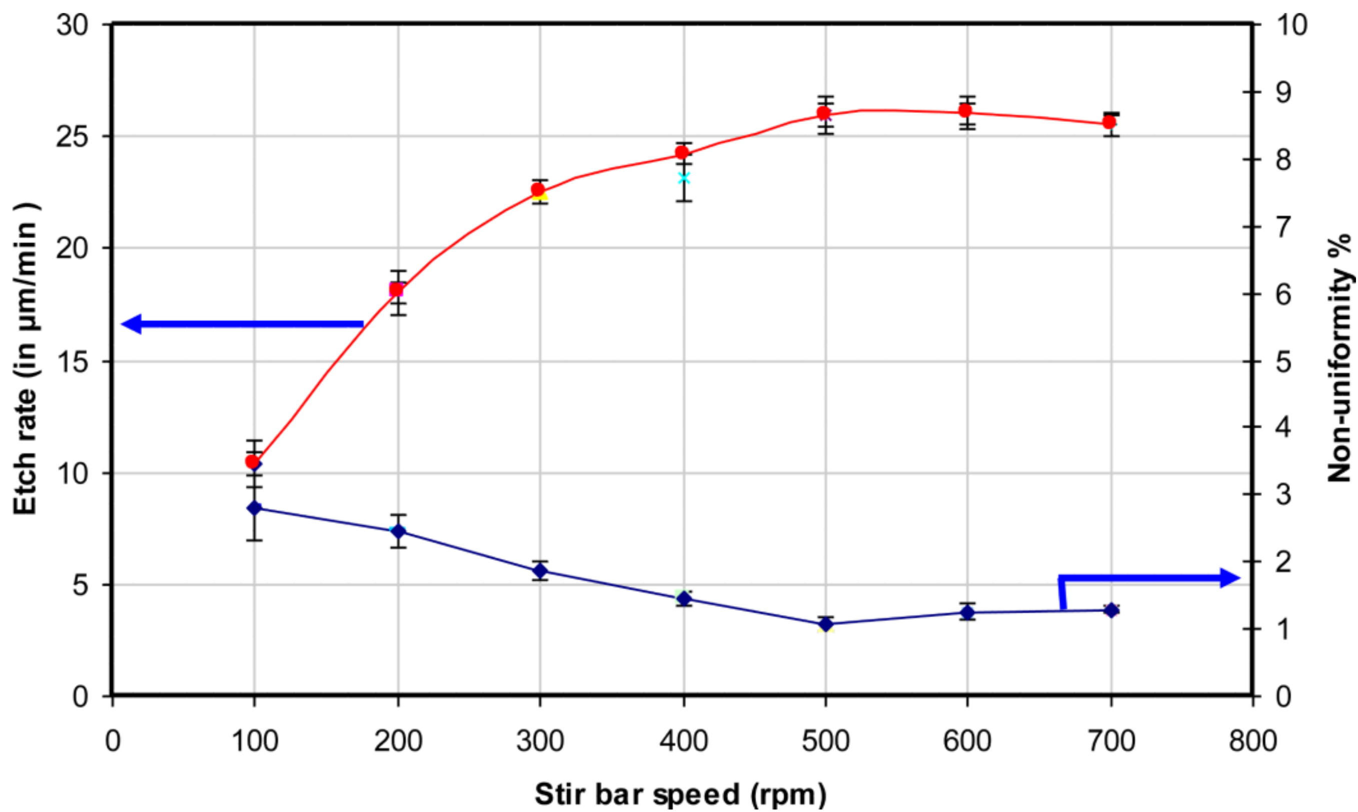

Fig. 6.
Plot of the column etch rate and non-uniformity in column width as a function of stir-bar speed. Each data point represents 3 etch experiments.

NIH-PA Author Manuscript
NIH-PA Author Manuscript
NIH-PA Author Manuscript

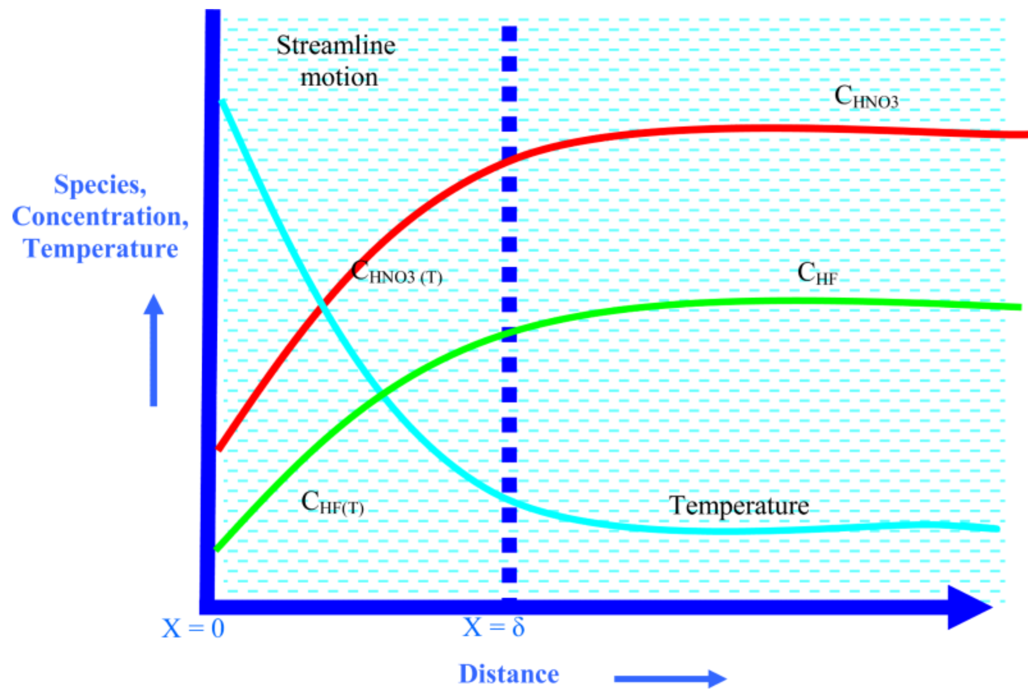

Fig. 7.

Model for reaction mechanism. Here x = 0 represents silicon surface. The plot has been adapted from Robbins and Schwartz's work on planar silicon surface [10-13] to explain the etching mechanism in the UEA.

NIH-PA Author Manuscript

NIH-PA Author Manuscript

NIH-PA Author Manuscript

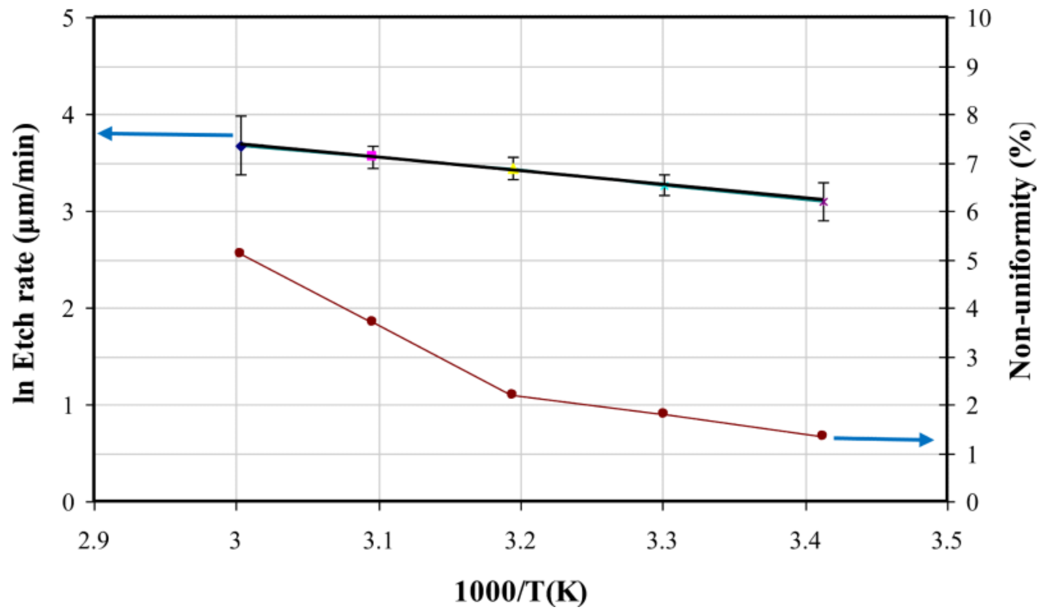

Fig. 8.
Arhenius plot of etch rate versus temperature and the non-uniformity (%) in tip geometry also as a function of temperature.

NIH-PA Author Manuscript
NIH-PA Author Manuscript
NIH-PA Author Manuscript

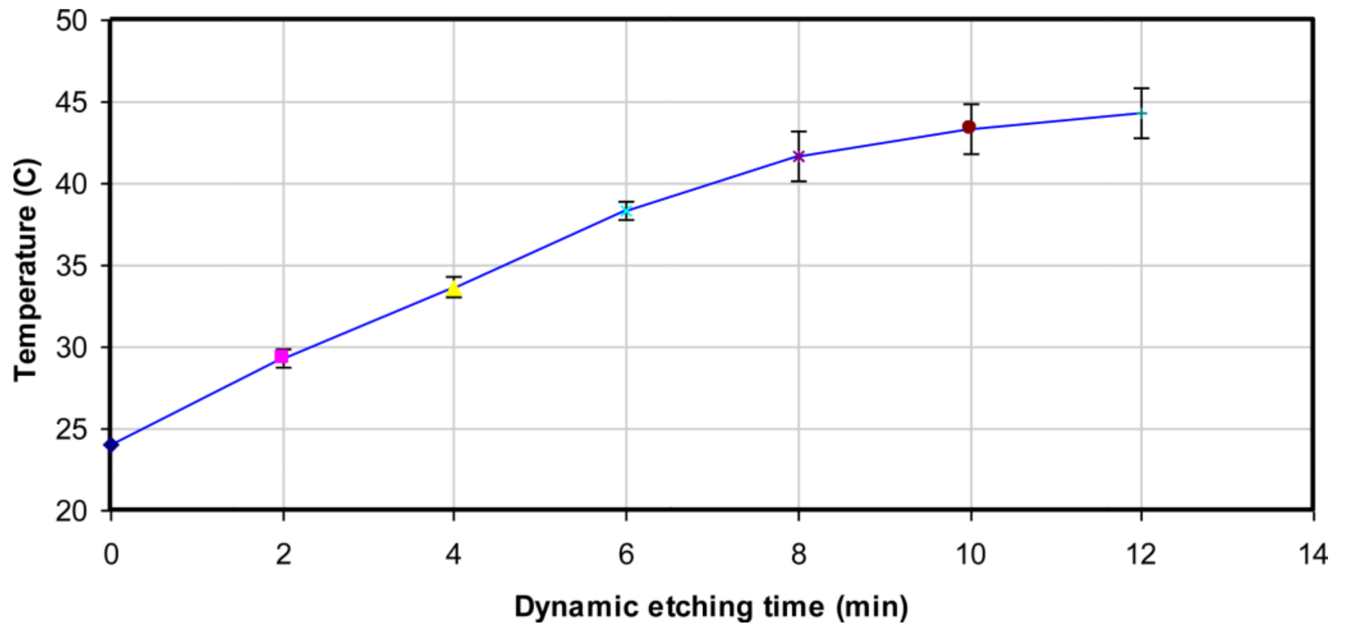

Fig. 9.
Plot of etching time versus temperature.

NIH-PA Author Manuscript

NIH-PA Author Manuscript

NIH-PA Author Manuscript

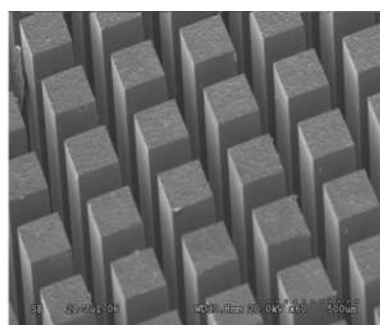

(a): After dicing

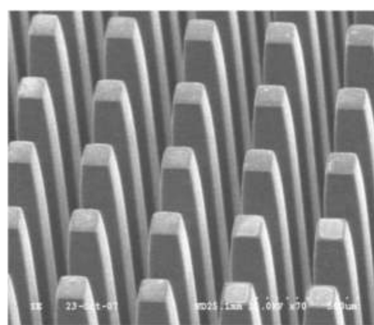

(b): After dynamic etching (t = 4 min)

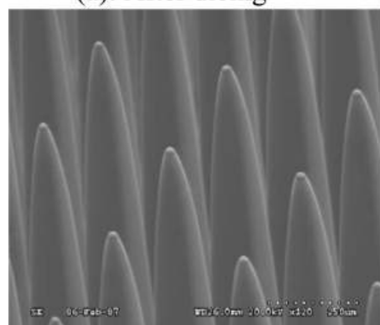

(c): During static etching (t = 7 min)

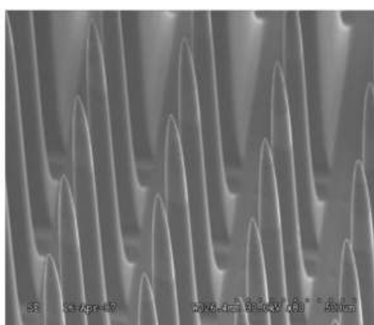

(d): After static etching (t = 8 min)

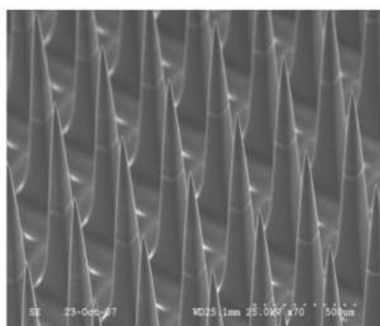

(e): After static over-etching (t = 8.3)

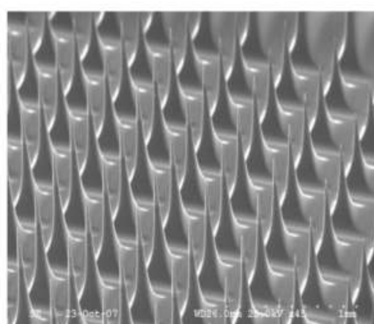

(f): After static over-etching (t = 9 min)

Fig. 10.

SEM images showing progression of electrode formation from dicing through etching (af). The rectangular columns (a) are transformed into sharp electrodes (d) during static etching (8 min). The high etch rate (20 um/min), causes significant change in the geometry of the electrodes. The etching time can be varied to achieve desired final electrode shape. The geometry can range from thick, rigid, “missile” shaped electrodes with a rounded or pointed tip to extremely thin, flexible electrodes.

NIH-PA Author Manuscript

NIH-PA Author Manuscript

NIH-PA Author Manuscript

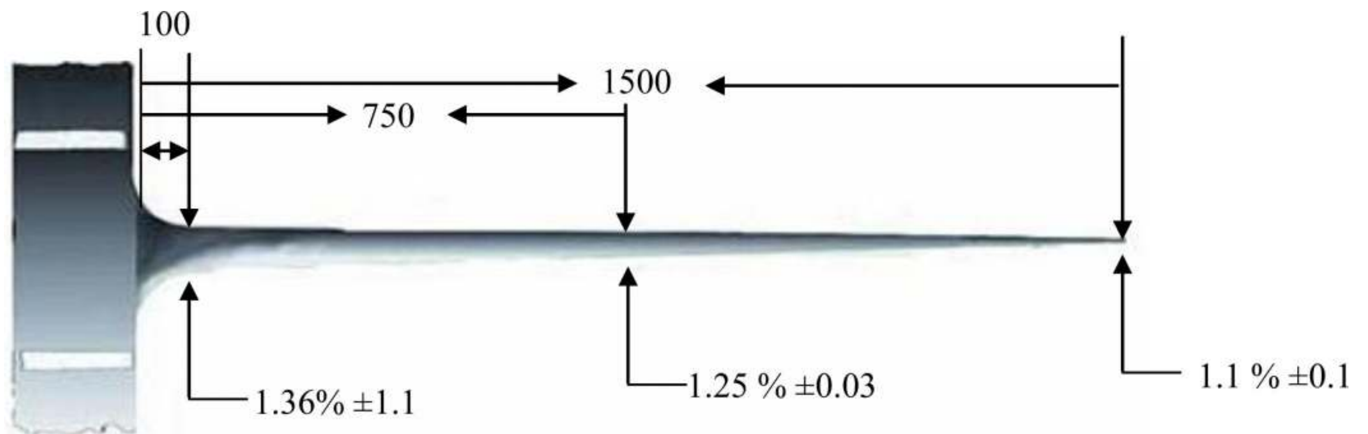

Fig. 11.
A scaled drawing of an electrode side view showing the distance from the electrode base at which all, measurement were made. Listed is the non-uniformity percentage ± the standard deviation for 350 electrodes measured from 5 wafers.

NIH-PA Author Manuscript
NIH-PA Author Manuscript
NIH-PA Author Manuscript

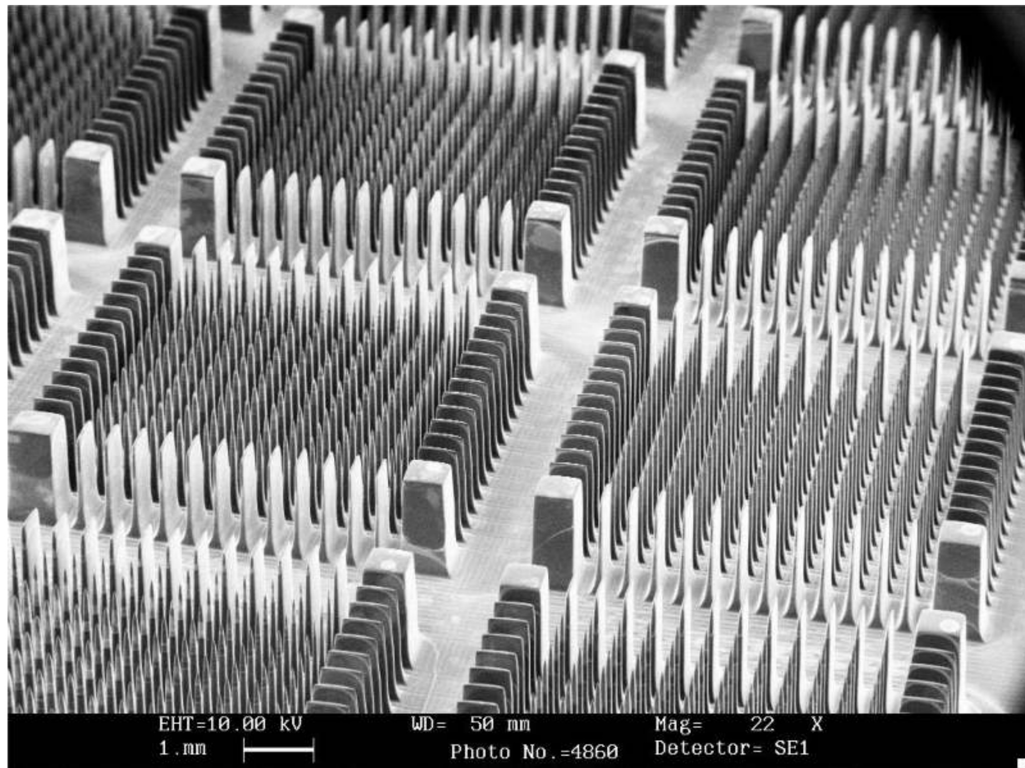

Fig. 12.
SEM micrograph of electrode arrays after *static* etching, performed on a 75 mm diameter wafer. Note the sacrificial features (extra row of electrodes, fins, corner posts) surrounding the UEA. These additional features help achieve uniformity in electrode geometry and later in tip exposure during photoresist coating [16].

NIH-PA Author Manuscript NIH-PA Author Manuscript NIH-PA Author Manuscript

Table 1

Optimized etching parameters

Etching	**Parameter**	**Optimized value**
***Dynamic* etching**	Wafer rotation rate	22 rpm
	Separation between stir-bar and wafer	2 inches
	Stir-bar rotation rate	500 rpm
	Etching time	4 min
***Static* etching**	Etching time	8 min

NIH-PA Author Manuscript NIH-PA Author Manuscript NIH-PA Author Manuscript

Table 2

Etching results

Electrode	**Average from five wafers**	**Non-uniformity within an array**	**Non-uniformity across five wafer**
After *dynamic* etching column width	122 ± 7μm	1.5 ± 0.5 %	2 ± 0.3 %
After *static* etching electrode length	1.3 mm	0.7 ± 0.2 %	1.02 ± 0.19 %